DALTON

Syntheses, structures and electrochemistry of $[CuL^1(L^R)]BF_4$ [L^1 = 3-{2,5-dimethoxyphenyl)-1-(2-pyridyl)pyrazole; L^R = tris(3-arylpyrazolyl)-hydroborate] and $[CuL^1_2][BF_4]_2$. Effects of graphitic interactions on the stability of an aryl radical cation †

Malcolm A. Halcrow,*[a] Eric J. L. McInnes,[b] Frank E. Mabbs,[b] Ian J. Scowen,[c] Mary McPartlin,[c] Harold R. Powell[a] and John E. Davies[a]

[a] *Department of Chemistry, University of Cambridge, Lensfield Road, Cambridge, UK CB2 1EW*
[b] *EPSRC CW EPR Service Centre, Department of Chemistry, University of Manchester, Oxford Road, Manchester, UK M13 9PL*
[c] *School of Applied Chemistry, University of North London, 166–220 Holloway Road, London, UK N7 8DB*

Reaction of potassium 3(5)-(2,5-dimethoxyphenyl)pyrazolate with 2-bromopyridine in diglyme (2,5,8-trioxanonane) at 130 °C for 3 d afforded 3-(2,5-dimethoxyphenyl)-1-(2-pyridyl)pyrazole (L^1) in 69% yield after an aqueous quench and recrystallisation from hexanes. Complexation of hydrated $Cu(BF_4)_2$ with 1 molar equivalent of L^1 and $K[L^R]$ in CH_2Cl_2 afforded $[CuL^1(L^R)]BF_4$ [L^R = tris(3-arylpyrazolyl)hydroborate: R = Ph **1**, 2-furyl **2**, 2-thienyl **3**, 4-tolyl **4**, 4-FC_6H_4 **5** or 4-$MeOC_6H_4$ **6**]. The single-crystal structures of **1**·0.5H_2O and **2**·2CH_2Cl_2 contain square-pyramidal complex cations with CuN_5 donor sets. Both structures show the presence of intramolecular graphitic interactions between the pendant dimethoxyphenyl group of L^1 and a R substituent from the L^R ligand. Treatment of $Cu(BF_4)_2$·xH_2O with 2 molar equivalents of L^1 in MeCN afforded $[CuL^1_2][BF_4]_2$ **7**, the single-crystal structure of which shows a tetrahedrally distorted planar geometry about the Cu^{2+} ion with additional 2.9 Å Cu · · · O contacts to the 2-methoxy groups of each ligand, which ^{1}H NMR data suggest are retained in CD_3CN solution. Complexes **1**–**7** contain a $\{d_{x^2-y^2}\}^1$ copper(II) centre according to solution UV/VIS and EPR spectroscopies, **1**–**6** remaining five-co-ordinate in CH_2Cl_2 solution. Voltammetric measurements in CH_2Cl_2–0.5 mol dm^{-3} $NBu^n_4PF_6$ at 293 K showed that $E_{\frac{1}{2}}$ for the L^1–$[L^1]^{\bullet+}$ oxidation associated with the dimethoxyphenyl group of L^1 is unperturbed by the graphitic interaction involving this group in **1**–**6**. However, for **1**, **4** and **5** this couple is chemically reversible at scan rates between 10 and 1000 mV s^{-1}; for **2**, **3** and **6** this process is partially obscured by an irreversible L^R ligand oxidation. For L^1 and **7**, this process is quasi-reversible or irreversible under the same conditions. Hence, the intramolecular graphitic interactions in complexes **1**, **4** and **5** may kinetically stabilise the dimethoxyphenyl radical cation against decomposition.

Several metalloenzymes are known to employ non-innocent aromatic amino acid residues as electron sinks, electron shuttles or free-radical reaction centres.[1,2] In several of these cases, such as galactose oxidase[3] and cytochrome c peroxidase,[4] the redox-active arene takes part in a graphitic interaction with a neighbouring residue. In galactose oxidase, for example, the non-innocent phenoxide ligand at the copper centre is stacked above a tryptophan indole ring,[5] whose role is unknown but which is integral to the function of the active site.[6] While it is reasonable to suspect that such an interaction might play a role in stabilising the arene radicals generated during catalysis by these enzymes, the nature and magnitude of this stabilisation are unclear. For galactose oxidase in particular, a substantial role in the lowering of the oxidation potential of the redox-active phenoxide ligand, which occurs at $E_{\frac{1}{2}}$ = +0.40 V *vs.* normal hydrogen electrode (NHE)[7] compared to +0.94 V for a 'normal' tyrosine residue,[8] has been attributed to this graphitic interaction by some authors.[9]

We describe here the syntheses, structures and properties of a series of complexes of formula $[CuL^1(L^R)]BF_4$ [L^1 = 3-(2,5-dimethoxyphenyl)-1-(2-pyridyl)pyrazole; L^R = tris(3-arylpyrazolyl)hydroborate], which exhibit an intramolecular graphitic interaction in the solid state between the redox-active dimethoxyphenyl substituent of L^1 and an aryl substituent from the L^R protecting group. Thus, by varying the nature of R, we have investigated the effect of graphitic stacking on the structural and redox chemistry of the pendant dimethoxyphenyl group in these complexes. The synthesis, molecular structure and electrochemistry of the homoleptic complex $[CuL^1_2][BF_4]_2$ are also discussed.

Results and Discussion

Syntheses and characterisation of L^1 and the mixed-ligand copper(II) complexes

Reaction of the potassium salt of 5-(2,5-dimethoxyphenyl)-pyrazole[10] with 2-bromopyridine in diglyme (2,5,8-trioxanonane), followed by an aqueous quench and recrystallisation from hot hexanes, yields the bidentate compound L^1 as a white solid (Scheme 1). Compound L^1 is isolated cleanly as a single isomer, which precedent suggests should be the less sterically hindered 1,3-disubstituted pyrazole, rather than the 1,5-disubstituted product.[11] Our attempts to confirm the regiochemistry of L^1 by ^{13}C NMR spectroscopy proved ambiguous, however. The magnitude of $^2J(C^{3/5}–H^4)$ has been employed as an indicator for the regiochemistry of *N*,*C*-disubstituted pyrazoles, 1,3-disubstituted pyrazoles having been proposed to exhibit $^2J(C^{3/5}–H)$ = 8–10 Hz and 1,5-disubstituted isomers 4–6 Hz.[12] For L^1, however, $^2J(C^{3/5}–H)$ = 6.5 Hz in $CDCl_3$ solution. While this is in principle an inconclusive result, we have previously observed that (crys-

† Based on the presentation given at Dalton Discussion No. 2, 2nd–5th September 1997, University of East Anglia, UK.

Non-SI unit employed: G = 10^{-4} T.

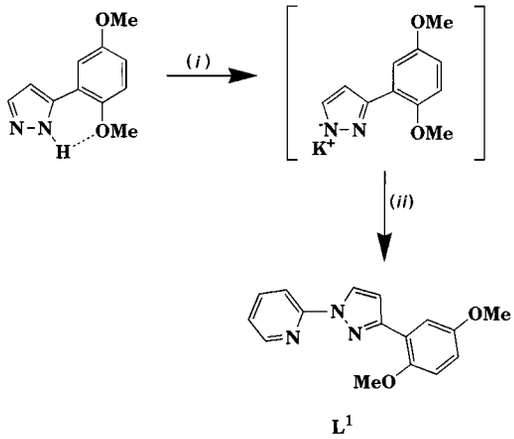

Scheme 1 (*i*) KH, diglyme, room temperature, N_2, 1 h; (*ii*) 2-bromopyridine, diglyme, 130 °C, 3 d; aqueous quench; recrystallisation from hexanes

tallographically characterised) 3-(ferrocenyl)-1-(2-pyridyl)pyrazole exhibits an identical value for this coupling.[13] We therefore suggested that L^1 was indeed the expected 1,3-disubstituted regioisomer, a proposal that was subsequently confirmed by the single-crystal X-ray diffraction studies of the copper(II) complexes of L^1 described below.

We originally selected L^{Ph} as a protecting ligand for the preparation of mixed-ligand complexes of L^1 because of its intermediate steric bulk[14] which has been previously employed to produce five-co-ordinate copper(II) complexes.[15] Treatment of $[Cu(O_2CMe)L^{Ph}]$[16] with 1 molar equivalent of L^1 and $NaBF_4$ in CH_2Cl_2 overnight at room temperature yields a deep green solution, from which dark green crystals of $[CuL^1(L^{Ph})]BF_4$ **1** can be isolated in *ca.* 70% yield by filtration, reduction of the filtrate to *ca.* 5 cm^3 volume and layering with Et_2O. Alternatively, direct reaction of $Cu(BF_4)_2 \cdot xH_2O$ ($x \approx 4$) with L^1 and $K[L^{Ph}]$[17] (1 : 1 : 1 molar ratios) in CH_2Cl_2 at room temperature for 1 h gives **1** in similar yield after an identical work-up and two recrystallisations to remove a small amount of copper(I) by-product. This latter procedure proved to be the method of choice for the general preparation of $[CuL^1(L^R)]BF_4$ complexes, because we were often unable to separate $[Cu(O_2CMe)L^R]$ starting materials containing other tris(3-arylpyrazolyl)hydroborates from contaminants derived from cleavage of the pyrazolylborate B–N bonds, a problem we have previously encountered in Cu/$[L^R]^-$ chemistry.[16] Thus, complexation of $Cu(BF_4)_2 \cdot xH_2O$ ($x \approx 4$) with L^1 and the known salts $K[L^R]$ (R = 2-thienyl,[18] 4-tolyl[19] or 4-methoxyphenyl[19]) or the new salts with R = 2-furyl or 4-fluorophenyl, which were synthesized by the usual procedures, yielded dark green crystals of $[CuL^1(L^R)]BF_4$ (R = 2-furyl **2**, 2-thienyl **3**, 4-tolyl **4**, 4-fluorophenyl **5** or 4-methoxyphenyl **6**) after an identical work-up to that employed for **1**.

Microanalytical data from complexes **1**–**6** are consistent with the proposed formulations, while FAB mass spectrometry in all cases gave $[^{63}CuL^1(L^R)]^+$ as the highest molecular ion (Table 1). The IR spectra of the complexes demonstrate the presence of L^1, BF_4^- and the relevant pyrazolylborate. While the solid-state IR spectra show some variation in ν(B–H), in CH_2Cl_2 solution for all the compounds this vibration appears at 2495 ± 3 cm^{-1} (Table 2) suggesting both that the solution structures of all these products are the same and that in the solid this vibration is strongly influenced by solid-state forces. The former conclusion is borne out by the UV/VIS and EPR data for these compounds (Tables 2 and 3), which are discussed below.

Similar complexation reactions to those employed for **1**–**6** involving $K[L^R]$ (R = H)[20] and $K[L^{R'}]$ [$L^{R'}$ = tris(3,5-dimethylpyrazolyl)hydroborate][21] yielded $[CuL^1_2][BF_4]_2$ **7** (see below) and $[CuL^R_2]$ (R = H)[22] or $[CuL^{R'}_2]$[23] only; the same products were isolated from reactions of $[\{Cu(\mu\text{-}Cl)L^R\}_2]$ (R = H)[24] with L^1 and $NaBF_4$. Interestingly, contamination by ligand-

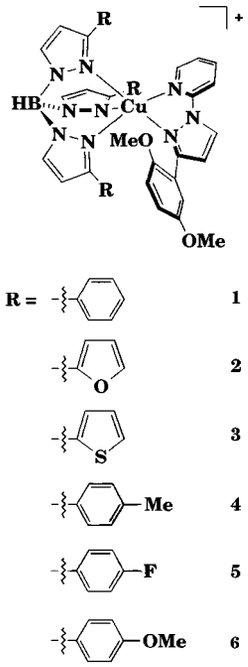

disproportionation products was not observed in the preparation of **2** or **3**, even though the 2-thienyl derivative is known readily to form octahedral $[ML^R_2]$ complexes.[18] With $K[L^R]$ (R = 2-pyridyl), the known complex $[Cu(OH_2)L^R]$[25] was obtained in high yield, no products containing L^1 being isolated.

Single-crystal structures of $[CuL^1(L^R)]BF_4$ (R = phenyl 1 or 2-furyl 2)

The single-crystal structures of complexes **1**·0.5H_2O and **2**·2CH_2Cl_2 confirm the proposed molecular geometry for these compounds. In both structures the Cu^{2+} ion exhibits a distorted square-pyramidal stereochemistry, with Cu–N distances within the usual range for such complexes[26] (Figs. 1–3, Table 4). There are two slight differences in the co-ordination environment at Cu between the two structures, however. First, the apical Cu–N bond for **2** [Cu–N(12) 2.241(4) Å] is slightly longer than that shown by **1** [2.209(4) Å]. This may reflect the steric demands of a dipolar interaction between the oxygen lone pair of the apical furyl group and the pyridyl ring of co-ordinated L^1 of **2** (Fig. 3), the distance from O(1) to the centroid of the pyridyl ring being 3.19 Å and the dihedral angle between the planes of the furyl and pyridyl groups being 65.7(3)°. Secondly, there are small differences in the angles within the basal planes of the two complex cations. This is best expressed by comparing the dihedral angle between the planes defined by Cu and the N donors of co-ordinated L^1 [N(41) and N(43)] and Cu and the two basal L^R N-donors [N(22) and N(32)] for the two structures; for **1** this angle is 13.1(3)°, while for **2** it is 7.3(3)°. This increased twist of L^1 relative to the pyrazolylborate ligand in **1** compared to that in **2** is probably a result of steric repulsions between the dimethoxyphenyl pendant and adjacent L^R R group in these structures, and reflects the increased bulk when R = Ph compared to R = 2-furyl, which should be sterically similar to R = 2-thienyl.[18]

The disposition of the pendant dimethoxyphenyl ring with respect to the Cu^{2+} ion is essentially the same in the two structures, the closest approach of this group to the copper ion being through the (unsubstituted) carbon atom at position 6 [for **1**, Cu · · · C(56) 3.696(5) Å; for **2**, Cu · · · C(56) 3.631(5) Å], while the two methoxy oxygen atoms are almost equidistant from the copper centre [for **1**, Cu · · · O(52) 5.585(4), Cu · · · O(55) 5.459(4) Å; for **2**, Cu · · · O(52) 5.569(4), Cu · · · O(55) 5.099(4) Å]. The orientation of the dimethoxyphenyl group

Table 1 Analytical and FAB mass spectrometric data for the copper complexes $[CuL^1(L^R)]BF_4$ **1**–**6** and $[CuL^1_2][BF_4]_2$ **7**

		Analysis (%)[a]			
Complex	R	C	H	N	*m*/*z*[b]
1·CH_2Cl_2	Ph	55.1 (55.2)	4.1 (4.1)	13.2 (13.2)	786, 642, 361
2·$2CH_2Cl_2$	2-Furyl	46.3 (46.3)	3.45 (3.5)	12.2 (12.4)	755, 622, 341
3	2-Thienyl	49.0 (49.9)	3.55 (3.5)	14.3 (14.2)	804, 654, 373
4·CH_2Cl_2	4-Tolyl	55.9 (56.4)	4.5 (4.55)	12.4 (12.6)	827, 670, 389
5·CH_2Cl_2	4-FC_6H_4	51.9 (52.2)	3.55 (3.6)	12.3 (12.5)	839, 678, 397
6	4-$MeOC_6H_4$	57.0 (57.4)	4.6 (4.5)	12.7 (13.1)	875, 702, 421
7	—	48.0 (48.1)	3.85 (3.8)	10.4 (10.5)	713, 625[c]

[a] Calculated values in parentheses. [b] Compounds **1**–**7** also exhibit *m*/*z* 344, 329 and 314 corresponding to $[^{63}CuL^1]^+$, $[^{63}CuL^1 - CH_3]^+$ and $[^{63}CuL^1 - 2CH_3]^+$. All peaks have correct isotopic distributions. Peaks for **1**–**6** are assigned to the ions $[^{63}CuL^1\{H^{11}B(N_2C_3H_2R)_3\}]^+$, $[^{63}CuL^1\{H^{11}B(N_2C_3H_2R)_2\}]^+$ and $[^{63}Cu\{H^{11}B(N_2C_3H_2R)_2\}]^+$, respectively. [c] Peaks are assigned to the ions $[^{63}CuL^1_2(^{11}BF_4)]^+$ and $[^{63}CuL^1_2]^+$, respectively.

Table 2 Infrared and UV/VIS spectroscopic data

	IR, $\tilde{\nu}$(B–H)/cm^{-1}		
Compound	Nujol	CH_2Cl_2	UV/VIS (CH_2Cl_2), λ_{max}/nm (ε_{max}/$dm^3\ mol^{-1}\ cm^{-1}$)
L^1	—	—	265 (sh), 280 (sh), 297 (15 900), 321 (14 700)
1	2485	2496	260 (sh), 316 (10 400), 360 (10 100), 463 (sh), 638 (107), 852 (sh)
2	2500	2493	261 (38 700), 286 (sh), 306 (sh), 356 (8900), 463 (sh), 625 (91), 864 (sh)
3	2480	2495	234 (sh), 263 (sh), 310 (sh), 360 (8400), 467 (sh), 626 (99), 852 (sh)
4	2513	2495	262 (sh), 314 (10 300), 360 (9800), 470 (sh), 639 (97), 854 (sh)
5	2504	2498	260 (sh), 314 (9300), 365 (8900), 472 (sh), 639 (103), 852 (sh)
6	2454	2495	247 (sh), 260 (42 700), 310 (sh), 360 (7600), 471 (sh), 633 (103), 873 (sh)
7*	—	—	206 (sh), 227 (sh), 261 (22 000), 296 (28 000), 318 (sh), 452 (sh), 717 (85), 892 (sh)

* The UV/VIS spectrum was obtained in MeCN solution.

Table 3 Frozen-solution EPR data [CH_2Cl_2–toluene (10 : 1), 120 K]

Complex	$g_\parallel$	$A_\parallel(^{63,65}Cu)$/G	$g_\perp$
1	2.250	165	2.056
2	2.245	172	2.062
3	2.246	170	2.055[a]
4	2.250	165	2.054
5	2.250	166	2.055
6	2.252	165	2.056
7[b]	2.273	147	2.089

[a] $A_\perp(^{14}N)$ = 14 G. [b] Spectrum run in MeCN–toluene (10 : 1).

relative to the Cu^{2+} ion is fixed by an intramolecular graphitic interaction with a R substituent of L^R. For **1**, the dihedral angle between the least-squares planes of the C(51)–C(56) and C(24)–C(29) phenyl groups is 6.5(3)°, while the distance between the centroid of the dimethoxyphenyl C_6 ring and the plane of the latter L^{Ph} phenyl group is 3.07 Å; for **2**, the parameters corresponding to the furyl group C(24)–C(27), O(2) are 5.4(3)° and 3.17 Å. The centroids of the dimethoxyphenyl and R groups in the two structures are offset by 3.0 (**1**, R = phenyl) and 2.9 Å (**2**, R = furyl), which are typical values for two graphitically interacting arenes.[27]

The relative orientations of the methoxy substituents on the dimethoxyphenyl group are different in the two structures. For complex **1**, the methoxy groups are transoid, with the C(58) oriented towards the apical pyrazole of the $[L^{Ph}]^-$ ligand, making a closest approach of 3.78 Å to N(12) of the pyrazole ring. This close contact causes C(58) to lie out of the plane of

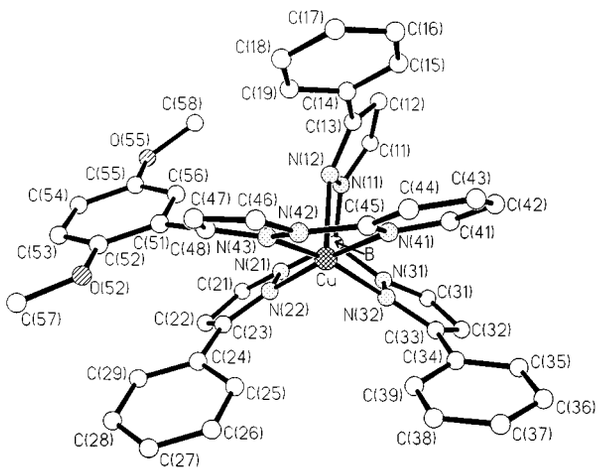

Fig. 1 Solid-state structure of the $[CuL^1(L^{Ph})]^+$ cation in the crystal of complex **1**·$0.5H_2O$, showing the atom numbering scheme employed. For clarity, all hydrogen atoms have been omitted

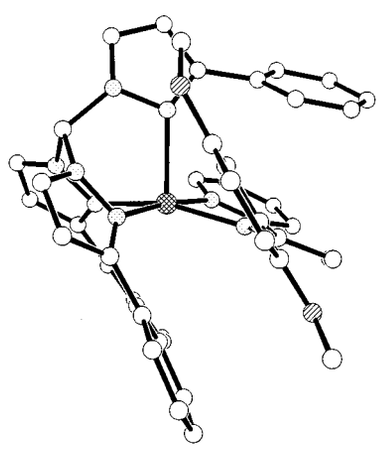

Fig. 2 Alternative view of the $[CuL^1(L^{Ph})]^+$ cation emphasising the geometry about the Cu^{2+} ion and the deviation of the O(55) methoxy group from the plane of the dimethoxyphenyl ring. For clarity, all hydrogen atoms have been omitted

the phenyl ring (Fig. 2), with a C(54)–C(55)–O(55)–C(58) torsion of 160.0(5)°. Similarly, the apical pyrazole group is bent away from this carbon atom, the plane of the pyrazole ring making an angle of 68.9(2)° with the least-squares plane formed by Cu, N(22), N(32) and B (Fig. 1). In **2**, the methoxy substituents are cisoid with the O(55) methoxy group oriented away from the 2-furyl L^R ligand, and neither of these distortions is present [the dihedral angle between the planes of the apical pyrazole and Cu, N(22), N(32) and B is 89.1(2)°; Fig. 3].

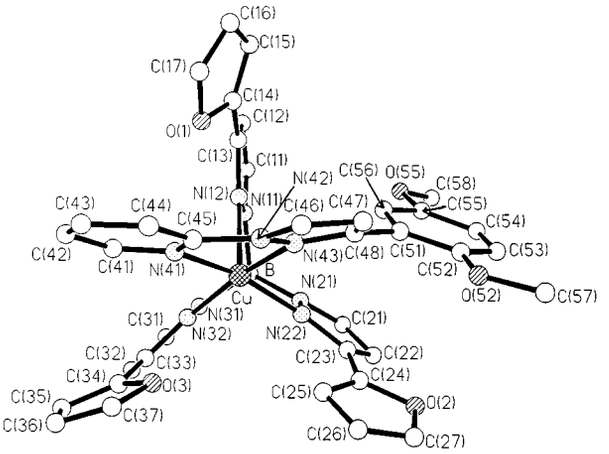

Fig. 3 Solid-state structure of the $[CuL^1(L^R)]^+$ (R = 2-furyl) cation in the crystal of complex **2**·$2CH_2Cl_2$. Details as in Fig. 1

Table 4 Bond lengths (Å) and angles (°) at copper for $[CuL^1(L^{Ph})]BF_4$·$0.5H_2O$ **1**·$0.5H_2O$ and $[CuL^1(L^R)]BF_4$·$2CH_2Cl_2$ **2**·$2CH_2Cl_2$ (R = 2-furyl)

	1·$0.5H_2O$	**2**·$2CH_2Cl_2$
Cu–N(12)	2.209(4)	2.241(4)
Cu–N(22)	1.995(4)	1.985(4)
Cu–N(32)	2.016(4)	2.019(4)
Cu–N(41)	2.018(4)	1.998(4)
Cu–N(43)	2.029(4)	2.023(4)
N(12)–Cu–N(22)	92.3(2)	94.2(2)
N(12)–Cu–N(32)	94.8(2)	91.3(2)
N(12)–Cu–N(41)	93.8(2)	99.89(14)
N(12)–Cu–N(43)	101.4(2)	99.5(2)
N(22)–Cu–N(32)	85.3(2)	83.7(2)
N(22)–Cu–N(41)	173.8(2)	165.9(2)
N(22)–Cu–N(43)	100.2(2)	97.4(2)
N(32)–Cu–N(41)	93.3(2)	96.3(2)
N(32)–Cu–N(43)	162.6(2)	168.9(2)
N(41)–Cu–N(43)	79.4(2)	79.91(14)

Synthesis and single-crystal structure of $[CuL^1_2][BF_4]_2$ 7

In addition to the mixed-ligand compounds, the homoleptic complex $[CuL^1_2][BF_4]_2$ **7** was also prepared so that its voltammetric properties could be compared with those of **1**–**6**. Direct complexation of $Cu(BF_4)_2$·xH_2O with 2 molar equivalents of L^1 in MeCN affords dark green blocks of **7** after vapour diffusion of Et_2O into the resultant solution. Analytical data were consistent with the formulation of **7** as the proposed homoleptic bis(ligand) dicationic complex, while IR and FAB mass spectrometry demonstrated the presence of L^1 and BF_4^- only (Table 1).

Attempts at a single-crystal X-ray analysis for complex **7** were persistently hampered by poor crystal quality, which was observed in data sets collected for both **7** and the corresponding PF_6^- salt at room and low temperatures. Attempts to prepare the BPh_4^- salt of the $[CuL^1_2]^{2+}$ dication, which might be expected to alleviate this problem, afforded instead its copper(I) congener.[28] Hence, the data for the single-crystal structure of **7** are relatively poor. However, the complex cation is free from disorder and is well defined, so that some discussion of its molecular geometry is justified. The two ligands form the expected tetrahedrally distorted planar arrangement about the copper ion with unexceptional Cu–N distances[26] (Fig. 4, Table 5), the dihedral angle (ω) between the least-squares planes of the two ligands being 41.4(2)°. The 2-methoxy groups of each ligand form a close contact to the same open face of the copper ion [Cu · · · O(20) 2.839(5), Cu · · · O(41) 2.929(5) Å, O(20) · · · Cu · · · O(41) 68.78(15)°]. These Cu · · · O interactions cause no appreciable displacement of the copper ion from the centre of the N_4 donor array, however.

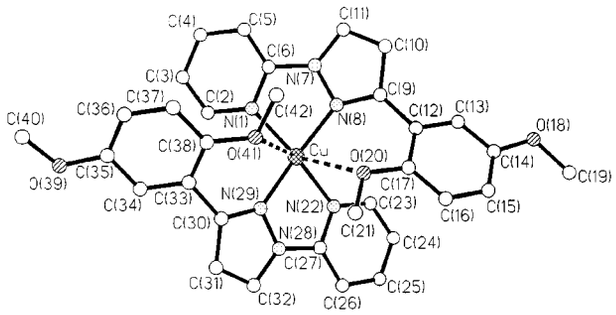

Fig. 4 Solid-state structure of the $[CuL^1_2]^{2+}$ dication in the crystal of complex **7**. Details as in Fig. 1

Table 5 Bond lengths (Å) and angles (°) at copper for $[CuL^1_2][BF_4]_2$ **7**

Cu–N(1)	1.992(5)	Cu–N(22)	1.997(6)
Cu–N(8)	1.974(5)	Cu–N(29)	1.961(5)
N(1)–Cu–N(8)	81.7(2)	N(8)–Cu–N(22)	105.7(2)
N(1)–Cu–N(22)	153.9(2)	N(8)–Cu–N(29)	152.7(2)
N(1)–Cu–N(29)	103.7(2)	N(22)–Cu–N(29)	81.3(2)

NMR, UV/VIS and EPR spectra of the complexes

The NMR spectra of copper(II) complexes have been little studied, because the long electron-spin relaxation time of the d^9 Cu^{2+} ion often broadens resonances from co-ordinated groups so severely as to be unobservable.[29] However, we and others[30] have found that ^{1}H NMR spectroscopy can be a useful structural probe for copper(II) centres. As a rule of thumb, we have found that protons more than four chemical bonds and >3 Å from a Cu^{2+} ion can be observed in a ^{1}H spectrum run under normal conditions. The 250 MHz ^{1}H spectrum of **1** in $CDCl_3$ exhibits the following peaks (Fig. 5): δ 11.9 (vbr), assigned to both the pyridyl H^4 proton of L^1 and the *o*-protons of the L^{Ph} phenyl rings; 8.0, 7.4, 7.2 (sh) and 5.7 (total integral 11.5 H), assigned to the *m*- and *p*-protons of phenyl, and the L^1 dimethoxyphenyl aryl hydrogens; and 3.9 and 3.0 (both 3 H), assigned to the two methoxy groups of L^1. An essentially identical spectrum was obtained for **1** in CD_3CN. These data are consistent with the solid-state structure of this compound, and demonstrate the absence of any close contacts or interactions between the Cu^{2+} ion and dimethoxyphenyl pendant in solution. The assignments of the spectrum of **1** were based on the ^{1}H NMR spectrum of **7** (see below), and the observations that $[Cu(bipy)_2][BF_4]_2$ (bipy = 2,2′-bipyridine)[31] exhibits a resonance at δ 12.3 in CD_3CN at 293 K,[32] and $[Cu(O_2CMe)L^{Ph}]$[16] shows peaks at δ 12.2 (vbr), 8.0 and 7.8 under the same conditions.[32] Proton NMR studies of **2**–**6** were hampered by their lower solubility in $CDCl_3$, which prevented the observation of some of the expected broader peaks in the aromatic region of the spectra; however, all of these compounds clearly exhibited two methoxy resonances with equal integrals, at δ 3.8–4.0 and 3.0–3.3.

The ^{1}H NMR spectrum of complex **7** in CD_3CN at 293 K shows, in addition to aromatic peaks at δ 12.9 (vbr), 7.6, 6.1 and 5.4 (approximate 1 : 1 : 1 : 1 integral ratios) which derive from the pyridyl H^4 and dimethoxyphenyl aryl protons, only one peak in the methoxy region of the spectrum at δ 3.6, which integrates to 3 : 1 against each of the aromatic peaks. This contrasts with the spectra of **1**–**6**, which exhibit two methoxy signals, and strongly suggests that the short Cu · · · O contacts observed for **7** in the

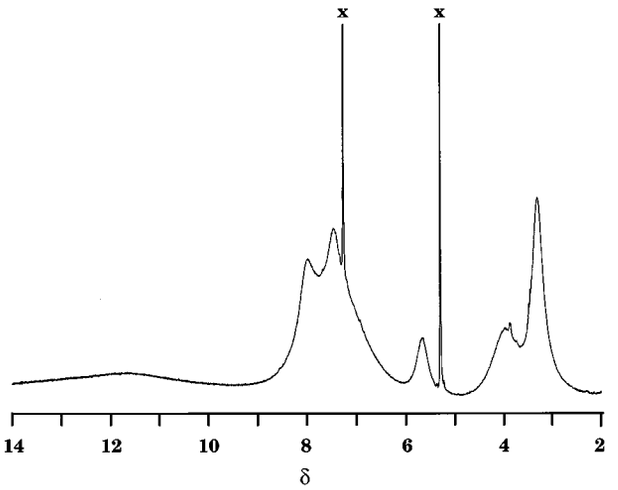

Fig. 5 Proton NMR spectrum of $[CuL^1(L^{Ph})]BF_4$ **1** in $CDCl_3$ (250 MHz, 293 K). X, residual $CHCl_3$ and CH_2Cl_2

crystal are maintained in this solvent, which would then render the methoxy groups adjacent to the Cu^{2+} ion unobservable.[30]

The UV spectrum of compound L^1 in CH_2Cl_2 at 293 K contains two absorption maxima at $\lambda_{max} = 297$ and 321 nm (Table 2). Although more intense, these are of comparable wavelength to those of two bands exhibited by 1,4-dimethoxybenzene,[33] and so can be assigned to $\pi \longrightarrow \pi^*$ transitions within the dimethoxyphenyl group of L^1. The spectrum also exhibits shoulders at 265 and 280 nm, which may arise from the pyrazolylpyridine fragment of the molecule [1-(2-pyridyl)pyrazole exhibits $\lambda_{max} = 250$ and 280 nm[34]].

The UV/VIS spectra of complexes **1**–**6** in CH_2Cl_2 at 293 K each show a d–d maximum bearing a high-wavelength shoulder in the range $\lambda_{max} = 625$–639 nm (ε_{max} *ca.* 100 $dm^3\ mol^{-1}\ cm^{-1}$, Table 2), as expected for a five-co-ordinate copper(II) complex with a $\{d_{x^2-y^2}\}^1$ ground state.[35,36] In addition, each of the complexes exhibit absorptions close to $\lambda_{max} = 260$ (sh), 315, 360 (both ε_{max} *ca.* 10 000 $dm^3\ mol^{-1}\ cm^{-1}$) and *ca.* 460 nm (sh, *ca.* 200), together with intense bands at low wavelength arising from intra-L^R $\pi \longrightarrow \pi^*$ transitions. The bands at 260 and 460 nm are also present in the spectrum of **7** (Table 2, see below), and are assigned to an intra-pyridyl $\pi \longrightarrow \pi^*$ transition from co-ordinated L^1[36] and a $Cu \rightarrow L^1$ metal-to-ligand charge-transfer (m.l.c.t.) transition,[36,37] respectively. However the other absorptions, which might be expected to be associated with the pendant dimethoxyphenyl group in these complexes, are substantially red-shifted from their positions in the spectra of free L^1 and **7**. It is unlikely that the transitions at 315 and 360 nm of complexes **1**–**6** correspond simply to excitonically shifted equivalents of the bands at 297 and 321 nm of free L^1, because the red-shifts involved (2000 and 3300 cm^{-1}, respectively) are greater than should be expected upon stacking of two monocyclic arenes (graphitic interactions between tetrapyrroles and organic dyes cause splittings or shifts of their $\pi \longrightarrow \pi^*$ transitions of up to 2000 cm^{-1}[38]). The assignment of these transitions, which in principal may incorporate interarene excitonic, charge resonance and/or charge-transfer processes,[38,39] is therefore unclear.

The EPR spectra of complexes **1**–**6** in CH_2Cl_2 : toluene (10 : 1) solution at 293 K were measured at both X- and S-band frequencies. The spectra obtained vary minimally between the complexes, showing $\langle g \rangle = 2.128 \pm 0.002$, $\langle A(^{63,65}Cu) \rangle = 60$ G and $\langle A(^{14}N) \rangle = 13$ G. The spectra exhibit severe m_I-dependent line broadening, so that at X-band the ^{14}N superhyperfine coupling is only resolved on the highest-field copper hyperfine line ($m_I = -\frac{3}{2}$). The S-band spectra show improved resolution of both the copper and nitrogen hyperfine interactions, however, the ^{14}N coupling now being resolved on both the $m_I = -\frac{1}{2}$ and $-\frac{3}{2}$ lines (Fig. 6). The X-band EPR spectra of **1**–**6** in the same solvent at 120 K exhibit the axial $g_\| > g_\perp$ pattern typical of tetragonal copper(II) centres[35,40] (Table 3). The spectra are almost identical for the six complexes, with **2** and **3** exhibiting slightly reduced $g_\|$ and increased $A_\|(^{63,65}Cu)$ values compared to those of the other samples. The spectra of **2**, **3** and **6** show features consistent with superhyperfine coupling to ^{14}N in the perpendicular region; for **3** only this was sufficiently resolved to give a measurable coupling constant of 14 G.

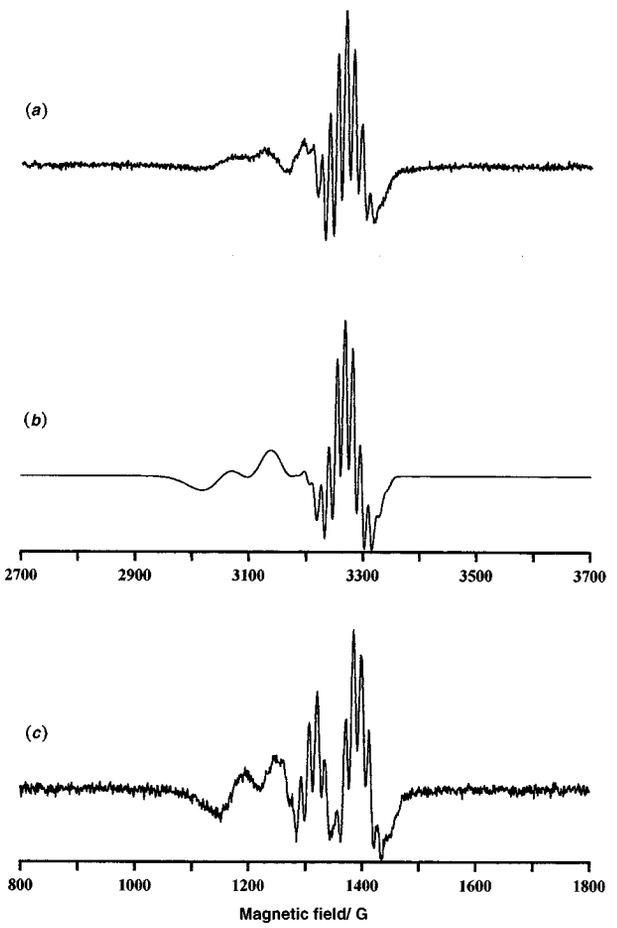

Fig. 6 Second-derivative EPR spectra of $[CuL^1(L^R)]BF_4$ **2** (R = 2-furyl) in CH_2Cl_2–toluene (10 : 1) solution at 298 K: (*a*) experimental X-band spectrum ($\nu = 9.438$ GHz); (*b*) simulation of (*a*) using $\langle g \rangle = 2.127$, $\langle A(^{63,65}Cu) \rangle = 60$ G, $\langle A(^{14}N) \rangle = 13$ G and linewidth coefficients $A = 40$ G, $B = 25$ G and $C = 0$ for the expression $\Delta B = A + Bm_I + Cm_I^2$, where ΔB is the peak-to-peak linewidth of the individual copper hyperfine lines; (*c*) experimental S-band spectrum ($\nu = 3.861$ GHz)

To address the question of whether ligand dissociation from complexes **1**–**6** occurs in solution, the second-derivative fluid solution EPR spectra of **2** were simulated assuming equal superhyperfine coupling to three, four or five ^{14}N nuclei (Fig. 7). The simulations involving four and five ^{14}N nuclei reproduce the main features of the spectrum equally well. However, the two high-field shoulders on the $m_I = -\frac{3}{2}$ line that are clearly resolved in the S-band spectrum (but not the X-band spectrum, Fig. 6) are *only* predicted for coupling to five ^{14}N centres. The ^{14}N superhyperfine constant derived from these calculations is unlikely to be accurate, since equal coupling to both basal and apical N nuclei of a square-pyramidal $[CuN_5]^{2+}$ centre is not chemically reasonable. However, the improved simulation obtained by assuming the presence of five rather than four or three ^{14}N nuclei is good evidence that the complexes remain five-co-ordinate in solution. Hence, taken together, the solution IR, UV/VIS, ^1H NMR and EPR spectroscopic data for **1**–**6** very strongly suggest that the solution

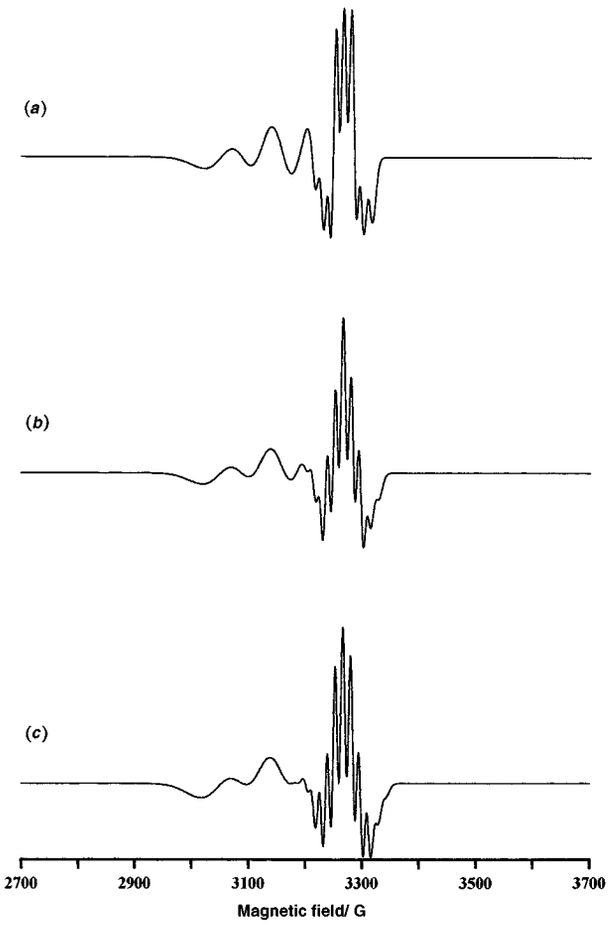

Fig. 7 Simulations of the second-derivative X-band EPR spectrum of complex **2** (Fig. 6) using the parameters given in the caption to Fig. 6. The simulations assume equal superhyperfine coupling to: (*a*) three; (*b*) four and (*c*) five ^{14}N nuclei

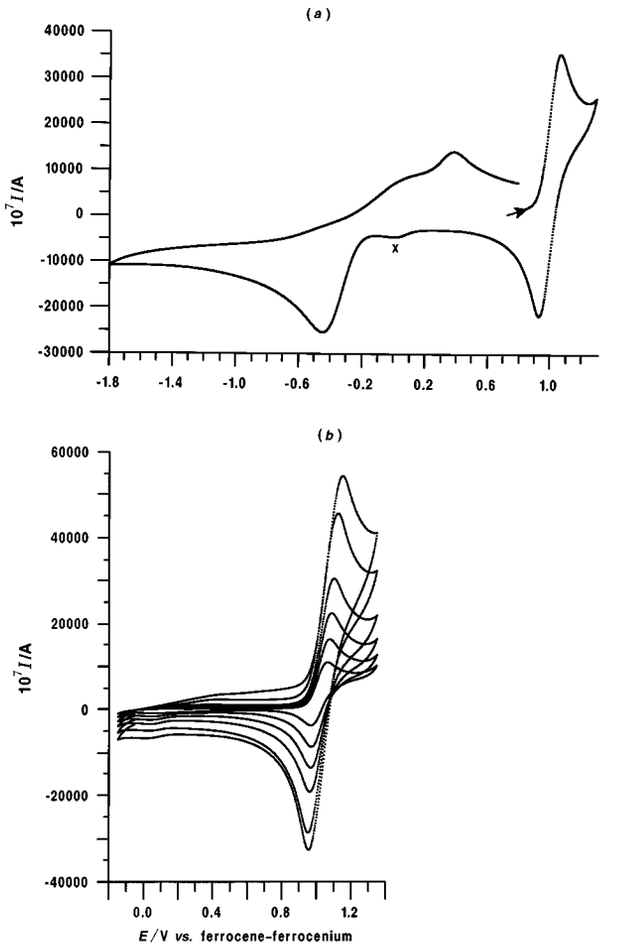

Fig. 8 Cyclic voltammograms of $[CuL^1(L^R)]BF_4$ (R = 4-fluorophenyl) **5** in CH_2Cl_2–0.5 mol dm^{-3} $NBu^n_4PF_6$ at 293 K: (*a*) scan rate 100 mV s^{-1}, omitting the irreversible $[L^R]^-$ ligand oxidation at +1.63 V. 'X' marks a weak daughter peak associated with the L^1–$[L^1]^{\bullet+}$ oxidation; (*b*) the L^1–$[L^1]^{\bullet+}$ oxidation at scan rates 10, 50, 100, 250, 750 and 1000 mV s^{-1}

and solid-state molecular structures of these compounds are essentially identical.

The d–d spectrum of complex **7** in MeCN is also consistent with a tetragonal $\{d_{x^2-y^2}\}^1$ ion and again shows an observable high-wavelength shoulder on the principal d–d maximum consistent with four- or five-co-ordination at Cu[34,35] (Table 2). The m.l.c.t. shoulder at 452 nm and intrapyridyl $\pi \longrightarrow \pi^*$ band at $\lambda_{max} = 261$ nm previously discussed for **1**–**6** are also present in this spectrum; in contrast to the mixed-ligand complexes, however, the dimethoxyphenyl-based $\pi \longrightarrow \pi^*$ absorptions are now almost unchanged in wavelength and absorption coefficient compared to uncomplexed L^1, occurring at $\lambda_{max} = 296$ and 318 nm. The shoulders in this spectrum at $\lambda < 230$ nm are probably associated with the pendant dimethoxyphenyl group.[33] The EPR spectra of **7** in MeCN–toluene (10:1) at 298 and 120 K are severely broadened: at 298 K, the spectrum consists of a broad, asymmetric resonance centred at $g_{app} = 2.107$ which is only slightly better resolved at S- compared to X-band frequencies, while at 120 K the expected axial $g_\| > g_\perp$ signal is observed, with no ^{14}N superhyperfine coupling being apparent (Table 3).

Electrochemical studies

Cyclic voltammetric (CV) data for L^1 and complexes **1**–**7** in CH_2Cl_2–0.5 mol dm^{-3} $NBu^n_4PF_6$ and MeCN–0.1 mol dm^{-3} $NBu^n_4PF_6$ at 293 K are listed in Table 6. The CVs of **1**–**7** are essentially invariant between these two solvents, with the proviso that the voltammograms obtained in MeCN exhibit somewhat broader waves, and for **1**–**6** contain additional weak irreversible features that could be taken to indicate partial ligand dissociation in this solvent. Unless otherwise stated, figures quoted in the text refer to data obtained in CH_2Cl_2.

The CV of compound L^1 in CH_2Cl_2–0.5 mol dm^{-3} $NBu^n_4PF_6$ at 293 K shows a quasi-reversible $[L^1]$–$[L^1]^{\bullet+}$ couple at $E_{\frac{1}{2}} = +0.90$ V *vs.* ferrocene–ferrocenium ($I_{p_c} : I_{p_a} = 0.4:1$ at scan rate $\nu = 100$ mV s^{-1}), with a major irreversible daughter product at $E_{p_c} = -0.75$ V. This oxidation wave contains shoulders at both low and high potentials, which may be ascribable to the presence of isomeric molecules bearing cisoid and transoid orientations of methoxy substituents[41] and/or to adsorption effects. The identity of the daughter product is unknown; while *o*-dimethoxybenzenes are known to form cyclic trimers upon electrooxidation,[42] no such products have been characterised for *p*-dimethoxybenzenes. 1,4-Dimethoxybenzene exhibits a similar oxidation at +1.34 V *vs.* saturated calomel electrode (SCE) in MeCN solution[41] (*ca.* +0.94 V *vs.* ferrocene–ferrocenium).

The CVs of complexes **1**–**6** under the same conditions also exhibit a one-electron L^1–$[L^1]^{\bullet+}$ oxidation, at $E_{\frac{1}{2}} = +0.98 \pm 0.03$ V (Fig. 8, Table 6), which now lacks fine structure. Interestingly, however, in CH_2Cl_2 for **1**, **4** and **5** this process is now chemically reversible at $10 \leqslant \nu \leqslant 1000$ mV s^{-1} [Fig. 8(*b*)] and retains its intensity upon repeated scanning, although this eventually results in the appearance of a weak irreversible daughter of unknown origin close to 0 V [Fig. 8(*a*)]. In MeCN, however, this couple, although chemically reversible when $\nu > 50$ mV s^{-1}, becomes quasi-reversible at very low scan rates ($I_{p_c} : I_{p_a}$ *ca.* 0.8:1

Table 6 Cyclic voltammetric data for the copper complexes in this study. All measurements were obtained in CH_2Cl_2–0.5 mol dm^{-3} $NBu^n_4PF_6$ or MeCN–0.1 mol dm^{-3} $NBu^n_4PF_6$ at 293 K under an argon atmosphere. Potentials are quoted *vs.* an internal ferrocene–ferrocenium standard, at a scan rate of 100 mV s^{-1}

Compound	Solvent	L^1–$[L^1]^{\cdot+}$ couple $E_{\frac{1}{2}}$/V (ΔE_p/mV; $I_{p_c}:I_{p_a}$)	L^R-based oxidation E_{p_a}/V	Cu^{II}–Cu^I reduction E_{p_c}/V (daughter E_{p_a}/V)
L^1	CH_2Cl_2	+0.90 (180; 0.4)	—	—
	MeCN	+0.93 (150; 0.4)	—	—
1	CH_2Cl_2	+0.97 (73; 1.0)	+1.59	−0.39 (+0.08, +0.38)
	MeCN	+0.97 (120; 1.0)	+1.67	−0.29 (+0.27)
2	CH_2Cl_2	+1.09[a]	+1.15	−0.48 (+0.07, +0.34)
	MeCN	+1.04[a]	+1.15	−0.51 (+0.33)
3	CH_2Cl_2	+1.00 (140; 0.8)	+1.23	−0.38 (−0.03, +0.32)
	MeCN	+1.06[a]	+1.16	−0.43 (+0.30)
4	CH_2Cl_2	+1.01 (77; 1.0)	+1.47	−0.46 (−0.06)
	MeCN	+0.99 (133; 1.0)	+1.67	−0.41 (+0.36)
5	CH_2Cl_2	+0.99 (113; 1.0)	+1.63	−0.48 (+0.03, +0.32)
	MeCN	+1.00 (112; 1.0)	+1.69	−0.29 (+0.33)
6	CH_2Cl_2	+0.95 (130; 0.2)	+1.17	−0.58 (+0.09)
	MeCN	+1.09[a]	+1.24	−0.42 (+0.29)
7	CH_2Cl_2	+1.06[a]	—	−0.07[b]
	MeCN	+1.03 (190; 0.3)	—	+0.08[b]

[a] Irreversible process, E_{p_a} value quoted. [b] Quasi-reversible process, $E_{\frac{1}{2}}$ value quoted.

at 10 mV s^{-1}), and slowly decays in intensity after repeated scanning; both these observations are consistent with the suggestion of increased ligand lability in this solvent. For **2**, **3** and **6** the L^1–$[L^1]^{\cdot+}$ wave is partially obscured by an irreversible L^R ligand oxidation (Table 6, see below), which causes partial or complete loss of reversibility of the L^1-based couple depending on the relative proximity of the two processes. In these cases the anodic peak potential for this process is very close to those exhibited by **1**, **4** and **5**, however.

In addition to the L^1-based oxidation, the voltammograms of complexes **1**–**6** also exhibit a one-electron irreversible reduction at a cathodic peak potential close to −0.4 V, that varies somewhat between compounds and solvents [Fig. 8(*a*), Table 6]. In CH_2Cl_2 this wave exhibits one or two daughters at E_{p_a} = *ca.* 0.0 and +0.3 V; in MeCN, only one daughter close to +0.3 V is observed. In both solvents, however, repeated scanning of the voltammogram in the range $+0.5 \leqslant E \leqslant -0.6$ V causes no decay in the intensities of these peaks, demonstrating the overall chemical reversibility of this electrochemical–chemical step reaction. We assign this reduction to the Cu^{II}–Cu^I couple, which would be expected to show behaviour of this type, since reduction of **1**–**6** should cause rapid decoordination of a L^R or L^1 N-donor to form a tetrahedral copper(I) species. No irreversible process ascribable to a Cu^I–Cu^0 reduction was detected. Finally, **1**–**6** show an irreversible L^R-based oxidation at more positive potentials (Table 6). Scanning past this oxidation in the CV destroys the return waves of the L^1 and Cu-based processes, indicating complete decomposition of the complexes.

The CV of complex **7** in CH_2Cl_2–0.5 mol dm^{-3} $NBu^n_4PF_6$ at 293 K at 100 mV s^{-1} exhibits an irreversible two-electron wave attributable to a L^1-based oxidation at E_{p_a} = +1.06 V, which becomes quasi-reversible at high scan rates ($E_{\frac{1}{2}}$ = +0.95 V, ΔE_p = 280 mV, $I_{p_c}:I_{p_a}$ = 0.2:1 at 500 mV s^{-1}). In contrast to **1**–**6**, this oxidation shows improved reversibility in MeCN–0.1 mol dm^{-3} $NBu^n_4PF_6$, being observed as a quasi-reversible process under these conditions ($E_{\frac{1}{2}}$ = +1.03 V, ΔE_p = 190 mV, $I_{p_c}:I_{p_a}$ = 0.3:1 at 100 mV s^{-1}). The voltammogram of **7** also contains a broad quasi-reversible reduction, occurring at $E_{\frac{1}{2}}$ = −0.07 V in CH_2Cl_2 and at +0.08 V in MeCN, which we ascribe to the Cu^{II}–Cu^I couple, and an irreversible process at E_{p_c} = −1.0 V with an associated desorption spike corresponding to a Cu^I–Cu^0 reduction. The former assignment was confirmed by treating a MeCN solution of **7** with ferrocene, which caused their immediate conversion into $[CuL^1_2]BF_4$[28] and $[Fe(cp)_2]BF_4$ (cp = η^5-C_5H_5) (identified by UV/VIS spectroscopy).

Discussion

Comparing the L^1–$[L^1]^{\cdot+}$ oxidations in the voltammograms exhibited by complexes **1**–**6** with those shown by L^1 and **7**, we make the following observations. First, $E_{\frac{1}{2}}(L^1$–$[L^1]^{\cdot+})$ for **1**–**6** is indistinguishable from that for **7**, within the limits of the voltammetric methods employed. Compared to **1**–**6**, the complex cation in **7** exhibits no graphitic interactions, an increased charge, lower co-ordination number at Cu and closer Cu · · · O contacts to the dimethoxyphenyl pendants; all of these factors in principle might raise the oxidation potential of the pendant dimethoxyphenyl groups in **7** on Coulombic or inductive grounds. Therefore, since $E_{\frac{1}{2}}(L^1$–$[L^1]^{\cdot+})$ is no less positive for **1**–**6** compared to **7**, it seems highly unlikely that the L^1/L^R stacking interaction in **1**–**6** confers any additional thermodynamic stabilisation on the dimethoxyphenyl radical cation oxidation products. This contrasts with a previous electrochemical study of cofacial porphyrins, which exhibited oxidation potentials ≤0.08 V (8 kJ mol^{-1}) lower than those of analogous porphyrin monomers.[43] However, while enthalpies of dimerisation for porphyrins and polycyclic arenes have been measured at 20–60 kJ mol^{-1},[44] the strength of such an interaction between two monocyclic arenes should be <10 kJ mol^{-1}.[45] Hence, it is not surprising that any perturbation of $E_{\frac{1}{2}}(L^1$–$[L^1]^{\cdot+})$ by such an interaction should be below the limits of reliable detection by voltammetry in our laboratory, which we estimate at 0.02 V or 2 kJ mol^{-1}.

Secondly, there is no apparent variation in $E_{\frac{1}{2}}(L^1$–$[L^1]^{\cdot+})$ between complexes **1**–**6**, despite the variation in L^R. This can be contrasted with the results of Cozzi *et al.*[46] who showed that substitution at the 4 position of one phenyl group in 1,8-diphenylnaphthalenes can increase the barrier to phenyl group rotation in these compounds by up to 15 kJ mol^{-1}, thus demonstrating that stacking interactions played a significant role in hindering this rotation. This suggests that if graphitic stacking thermodynamically stabilised $[L^1]^{\cdot+}$ then changing L^R might also be expected to cause a measurable variation in $E_{\frac{1}{2}}$. That it does not also implies that any perturbation of the energy of the L^1–$[L^1]^{\cdot+}$ couple by the graphitic interaction is very weak.

Thirdly, those complexes in which the L^R-based oxidation is sufficiently positive not to overlap with the L^1–$[L^1]^{\cdot+}$ wave exhibit a major increase in reversibility for the L^1-based oxidation compared to free L^1 and complex **7**, implying that the co-ordinated $[L^1]^{\cdot+}$ radical cation is kinetically stabilised. This is unlikely to reflect steric protection of the L^1 dimethoxyphenyl ring by the bulky L^R protecting ligands, since space-filling

models of complexes **1** and **2** show that the face of this arene that does not take part in the graphitic interaction is fully exposed to the environment. Therefore, the observed kinetic stabilisation may be a consequence of the L^1/L^R graphitic interaction. This is not unreasonable, since oxidation of a graphitically stacked arene to a cation radical might be expected to enhance interarene charge transfer and thus increase the π-stacking interaction. This strengthened graphitic interaction would then impose an increased activation barrier for decomposition of the interacting radical. Support for this suggestion is provided by the recent structural characterisation of the partially oxidised metalloporphyrin dimers $[\{M(oep^{\bullet/2})\}_2]^+$ (M = Ni or Cu; H_2oep = 2,3,7,8,12,13,17,18-octaethylporphyrin), which show shortened intradimer separations in the solid state compared to their neutral congeners.[47]

To conclude, we have shown that a graphitic interaction involving a redox-active arene in a well characterised series of copper(II) complexes imparts no measurable additional thermodynamic stability to the oxidised aryl radical cation. We therefore suggest that the tyrosine/tryptophan graphitic interaction in galactose oxidase,[3] which should be of a similar magnitude,[45a] will also contribute minimally to the lowered oxidation potential of the non-innocent phenoxide in this enzyme, and that other explanations for the unusual properties of this residue should be sought. Our results do suggest an alternative function for the galactose oxidase tyrosine/tryptophan stacking interaction, however, namely the kinetic stabilisation of this extremely long-lived phenoxyl radical. Experiments designed to examine in more detail the effects of graphitic interactions on the redox properties of non-innocent organics are in progress in this laboratory.

Experimental

Unless stated otherwise, all manipulations were performed in air using commercial grade solvents. The compound diglyme was dried over sodium before use. 5-(2,5-Dimethoxyphenyl)-pyrazole,[10] the salts $K[L^R]$ (R = H,[20] Ph,[17] 2-thienyl,[18] 4-tolyl,[19] 4-methoxyphenyl,[19] or 2-pyridyl[48]), $K[L^{R'}]$,[21] $[Cu(O_2CMe)(L^{Ph})]$[16] and $[\{Cu(\mu\text{-}Cl)L^R\}_2]$[24] (R = H) were prepared by the literature procedures. [N.B. We have found the 1,3-dione intermediate in the preparation of 3(5)-(4-methoxyphenyl)pyrazole from 4-methoxyacetophenone[19] to be moderately photosensitive; appropriate precautions should be taken when attempting this synthesis.] 4-Fluoroacetophenone, 2-acetylfuran, dimethylformamide dimethyl acetal (Avocado), 2-bromopyridine, KH (40% w/w suspension in mineral oil) and $Cu(BF_4)_2{\cdot}xH_2O$ ($x \approx 4$; Aldrich) were used as supplied.

Syntheses

3(5)-(2-Furyl)pyrazole. 2-Acetylfuran (50 g, 0.45 mol) and dimethylformamide dimethyl acetal (80 g, 0.67 mol) were refluxed under N_2 for 16 h, yielding a dark red solution which was evaporated to dryness. The resultant orange solid was dissolved in $N_2H_4{\cdot}H_2O$ (45 g, 0.90 mol) and MeOH (75 cm^3), and the mixture refluxed for 1 h. The cooled red solution was poured onto ice, diluted to 1 l with water and left at 0 °C overnight. The yellow solid was filtered off, washed with water and dried *in vacuo*. Two recrystallisations from CH_2Cl_2 gave colourless microcrystals. Yield 37 g, 61% (Found: C, 62.6; H, 4.5; N, 20.7. Calc. for $C_7H_6N_2O$: C, 62.7; H, 4.5; N, 20.9%). M.p. 106–108 °C. Electron impact (EI) mass spectrum: *m*/*z* 134 (M^+), 105 ($[M - CHO]^+$) and 79 ($[M - C_3H_3O]^+$). NMR spectra ($CDCl_3$, 293 K): ^{1}H, δ 12.97 (br, 1 H, NH), 7.66 (d, 1 H, *J* 2.3, pz $H^{5(3)}$), 7.47 (d, 1 H, *J* 1.8, furyl H^5), 6.65 (d, 1 H, *J* 3.3, furyl H^3), 6.54 (d, 1 H, *J* 2.3, pz H^4) and 6.48 (dd, 1 H, *J* 1.8 and 3.3 Hz, furyl H^4); ^{13}C, δ 148.4 (furyl C^2), 141.9 (furyl C^5), 131.8 (pz $C^{5(3)}$), 111.5 (furyl C^4), 106.1 (furyl C^3) and 102.1 (pz C^4); pz $C^{3(5)}$ not observed. IR (Nujol): 3149m cm^{-1} (N–H).

K[L^R] (R = 2-furyl). A mixture of 3(5)-(2-furyl)pyrazole (20 g, 0.15 mol) and KBH_4 (2.0 g, 0.037 mol) was heated to 200 °C for 2 h, until the mixture resolidified. The product was washed with boiling toluene and hexanes, to yield a mildly photosensitive white solid that was analysed without further purification. Yield 12.6 g, 56% (Found: C, 55.4; H, 3.55; N, 18.4. Calc. for $C_{21}H_{16}BKN_6O_3$: C, 56.0; H, 3.6; N, 18.7%). Negative-ion FAB mass spectrum: *m*/*z* 411 ($[L^R]^-$). NMR spectra (CD_3CN, 293 K): ^{1}H, δ 7.65 (d, 3 H, *J* 2.2, pz H^5), 7.46 (dd, 3 H, *J* 0.8 and 1.8, furyl H^5), 6.54 (dd, 3 H, *J* 0.8 and 3.3, furyl H^3), 6.45 (dd, 3 H, *J* 1.8 and 3.3, furyl H^4), 6.35 (d, 3 H, *J* 2.2 Hz, pz H^4); ^{13}C, δ 151.4, 145.0 (furyl C^2 + pz C^3), 142.2 (furyl C^5), 136.7 (pz C^5), 111.9 (furyl C^4), 105.3 (furyl C^3) and 101.5 (pz C^4). IR (Nujol): 2400w cm^{-1} (B–H).

3(5)-(4-Fluorophenyl)pyrazole. Method as for 3(5)-(2-furyl)-pyrazole, using 4-fluoroacetophenone (62 g, 0.45 mol) as starting material. The product formed large colourless needles from CH_2Cl_2–hexanes. Yield 47 g, 64% (Found: C, 66.7; H, 4.4; N, 17.1. Calc. for $C_9H_7FN_2$: C, 66.7; H, 4.35; N, 17.3%). M.p. 103–105 °C. EI mass spectrum: *m*/*z* 162 (M^+). NMR spectra ($CDCl_3$, 293 K): ^{1}H, δ 7.73 (dd, 2 H, *J* 5.6 and 8.9, Ph $H^{2/6}$), 7.59 (br, 1 H, pz $H^{5(3)}$), 7.07 (t, 2 H, *J* 8.9, Ph $H^{3/5}$) and 6.56 (br, 1 H, pz H^4); ^{13}C, δ 162.7 (d, *J* 247, Ph C^4), 149.4 (pz $C^{3(5)}$), 132.5 (pz $C^{5(3)}$), 128.7 (Ph C^1), 127.5 (d, *J* 8, Ph $C^{2/6}$), 115.7 (d, *J* 22 Hz, Ph $C^{3/5}$) and 102.5 (pz C^4); ^{19}F, δ −114.4 (br). IR (Nujol): 3124m cm^{-1} (N–H).

K[L^R] (R = 4-fluorophenyl). A mixture of 3(5)-(4-fluorophenyl)pyrazole (20 g, 0.14 mol) and KBH_4 (1.9 g, 0.035 mol) in anisole (50 cm^3) was refluxed for 3 d. The cloudy solution was allowed to cool, resulting in the precipitation of feathery white needles which were filtered off, washed with hot toluene and hexanes, and dried *in vacuo*. The product contained some toluene and *ca*. 5% unreacted pyrazole according to ^{1}H NMR spectroscopy, but was sufficiently pure for complex synthesis. Yield 12.0 g, 48% (Found: C, 59.0; H, 3.6; N, 15.0. Calc. for $C_{27}H_{19}BF_3KN_6$: C, 60.7; H, 3.6; N, 15.7%). Negative-ion FAB mass spectrum: *m*/*z* 495 ($[L^R]^-$). NMR spectra (CD_3CN, 293 K): ^{1}H, δ 7.78 (dd, 6 H, *J* 5.6 and 8.9, Ph $H^{2/6}$), 7.63 (d, 3 H, *J* 2.2, pz H^5), 7.07 (t, 6 H, *J* 8.9, Ph $H^{3/5}$) and 6.47 (d, 3 H, *J* 2.2 Hz, pz H^4); ^{13}C, δ 162.7 (d, *J* 242, Ph C^4), 151.6 (pz C^3), 136.5 (pz C^5), 132.8 (Ph C^1), 128.0 (d, *J* 8, Ph $C^{2/6}$), 115.9 (d, *J* 22, Ph $C^{3/5}$) and 101.9 (pz C^4); ^{19}F, δ −117.0 (tt, *J* 8.9 and 5.6 Hz). IR (Nujol): 2408w cm^{-1} (B–H).

3-(2,5-Dimethoxyphenyl)-1-(2-pyridyl)pyrazole (L^1). A mixture of 5-(2,5-dimethoxyphenyl)pyrazole (10.0 g, 0.049 mol) and KH (2.0 g, 0.049 mol) was stirred in diglyme (60 cm^3) under N_2 for 1 h, giving a gelatinous white precipitate. 2-Bromopyridine (7.8 g, 0.049 mol) was then added, and the mixture stirred under N_2 at 130 °C for 3 d. The solution was quenched with an equal volume of water and refrigerated overnight. The resultant pale yellow solid was filtered off and dried over P_2O_5. Recrystallisation from hot hexanes yielded white plates. Yield 9.5 g, 69% (Found: C, 68.5; H, 5.45; N, 15.1. Calc. for $C_{16}H_{15}N_3O_2$: C, 68.3; H, 5.35; N, 14.9%). M.p. 74–76 °C. EI mass spectrum: *m*/*z* 281 (M^+), 266 ($[M - CH_3]^+$), 252 ($[M - 2CH_3 + H]^+$), 203 ($[M - C_5H_5N]^+$), 188 ($[M - C_5H_5N - CH_3]^+$) and 78 ($[C_5H_5N]^+$). NMR spectra ($CDCl_3$, 293 K): ^{1}H, δ 8.60 (d, 1 H, *J* 2.6), 8.38 (ddd, 1 H, *J* 4.9, 1.8 and 0.9), 8.10 (d, 1 H, *J* 8.3), 7.80 (ddd, 1 H, *J* 8.3, 7.4 and 1.8), 7.70 (d, 1 H, *J* 2.5), 7.15 (ddd, 1 H, *J* 7.4, 4.9 and 0.9), 7.05 (d, 1 H, *J* 2.6), 6.93 (d, 1 H, *J* 8.8), 6.86 (dd, *J* 8.8 and 2.5 Hz, 1 H), 3.87 (s, 3 H) and 3.85 (s, 3 H); ^{13}C, δ 153.8, 151.7, 151.6, 150.8 (py C^2 + pz C^3 + Ph C^2 and C^5), 148.0 (py C^6), 138.6 (py C^4), 127.4 (pz C^5), 122.6 (Ph C^1), 121.2, 114.9 (py C^3 and C^5), 113.7, 113.0, 112.5 (Ph C^3, C^4 and C^6), 109.6 (pz C^4), 56.2 (OCH_3) and 55.8 (OCH_3).

[3-(2,5-Dimethoxyphenyl)-1-(2-pyridyl)pyrazole][hydridotris-(3-phenylpyrazolyl)borato]copper(II) tetrafluoroborate 1. *Method* 1. The complex $[Cu(O_2CMe)L^{Ph}]$ (0.30 g, 5.34×10^{-4} mol), L^1

Table 7 Experimental details for the single-crystal structure determinations of $[CuL^1(L^{Ph})]BF_4\cdot0.5H_2O$ **1**·0.5H_2O, $[CuL^1(L^R)]BF_4\cdot2CH_2Cl_2$ **2**·2CH_2Cl_2 (R = 2-furyl) and $[CuL^1_2][BF_4]_2$ **7**

	1·0.5H_2O	**2**·2CH_2Cl_2	**7**
Formula	$C_{43}H_{38}B_2CuF_4N_9O_{2.5}$	$C_{39}H_{35}B_2Cl_4CuF_4N_9O_5$	$C_{32}H_{30}B_2CuF_8N_6O_4$
M_r	881.98	1012.72	779.78
Crystal habit	Dark green prism	Dark green block	Dark green lath
Crystal size/mm	0.40 × 0.15 × 0.10	0.36 × 0.20 × 0.16	0.36 × 0.10 × 0.04
Crystal class	Monoclinic	Triclinic	Monoclinic
Space group	$P2_1/c$	$P\bar{1}$	$P2_1/n$
a/Å	12.867(8)	12.1339(5)	14.077(3)
b/Å	14.600(12)	12.6535(4)	15.215(3)
c/Å	22.331(7)	17.071(2)	17.767(2)
α/°	—	102.163(6)	—
β/°	95.76(4)	99.067(6)	108.891(12)
γ/°	—	115.747(5)	—
U/Å^3	4179.6(15)	2213.6(3)	3600.6(11)
Z	4	2	4
D_c/Mg m^{-3}	1.400	1.519	1.475
Radiation (λ/Å)	Mo-Kα (0.710 73)	Cu-Kα (1.541 78)	Mo-Kα (0.710 69)
No. reflections for lattice parameters	25	40	25
θ Range for lattice parameters/°	15.0–20.0	11.0–28.0	12.9–17.7
μ/mm^{-1}	0.591	3.534	0.693
F(000)	1813	1030	1628
T/K	153(2)	297(2)	293(2)
Diffractometer	Rigaku AFC7R	Siemens P4	Rigaku AFC5R
Scan type	ω–2θ	θ–2θ	ω–2θ
Minimum, maximum transmission	0.80, 1.00	0.49, 0.72	0.84, 1.00
Measured reflections	8842	11 570	9948
Independent reflections	6715	5790	8255
R_{int}	0.0555	0.0388	0.0528
Observed reflections [$I > 2\sigma(I)$]	4478	4342	3220
θ Range/°	3–25	3–57	2–28
Standards	3 every 200 reflections	3 every 97 reflections	3 every 150 reflections
Variation (%)	1	4	0.4
hkl Ranges	0–14, 0–16, −26 to 25	−13 to 13, −12 to 12, −18 to 18	−1 to 18, −1 to 19, −23 to 22
No. parameters	587	590	502
No. restraints	12	0	12
R(*F*)	0.0603	0.0566	0.0824
wR(F^2)	0.1692	0.1439	0.2896
S	1.085	1.030	1.024
Weighting scheme, w^{-1}	$\sigma^2(F_o^2) + (0.0439P)^2 + 8.9805P$	$\sigma^2(F_o^2) + (0.0578P)^2 + 2.8697P$	$\sigma^2(F_o^2) + (0.1387P)^2$
$\Delta\rho_{min}$, $\Delta\rho_{max}$/e Å^{-3}	−0.495, 0.779	−0.504, 0.493	−0.893, 0.865

Semiempirical absorption correction (ψ scans). $R = \Sigma[|F_o| - |F_c|]/\Sigma|F_o|$, $wR = [\Sigma w(F_o^2 - F_c^2)/\Sigma wF_o^4]^{\frac{1}{2}}$, $P = (F_o^2 + 2F_c^2)/3$.

(0.15 g, 5.34×10^{-4} mol) and $NaBF_4$ (0.06 g, 5.34×10^{-4} mol) were stirred in CH_2Cl_2 at room temperature for 16 h, giving a deep green solution and white precipitate which was filtered off. Reduction of the filtrate to *ca*. 5 cm^3 volume and layering with Et_2O gave dark green blocks. Yield 0.35 g, 68%.

Method 2. A mixture of $K[L^{Ph}]$ (0.26 g, 5.34×10^{-4} mol), L^1 (0.15 g, 5.34×10^{-4} mol) and $Cu(BF_4)_2\cdot xH_2O$ (0.17 g, 5.34×10^{-4} mol) was stirred in CH_2Cl_2 (20 cm^3) at room temperature for 1 h. The resultant dark green solution was filtered, reduced to *ca*. 5 cm^3 volume, and layered with Et_2O. One further recrystallisation from CH_2Cl_2–Et_2O yielded dark green blocks in analytical purity. Yield 0.33 g, 65%.

Other [3-(2,5-dimethoxyphenyl)-1-(2-pyridyl)pyrazole][hydridotris(pyrazolyl)borato]copper(II) tetrafluoroborate complexes 2–6. Method 2 as described for complex **1** was followed exactly, substituting the relevant amount of the corresponding potassium pyrazolylborate precursor. Compound **3** only was recrystallised from MeCN, because of its lower solubility in CH_2Cl_2. Recrystallised yields ranged from 55 to 70%.

Bis[3-(2,5-dimethoxyphenyl)-1-(2-pyridyl)pyrazole]copper(II) bis(tetrafluoroborate) 7. A solution of L^1 (0.15 g, 5.34×10^{-4} mol) and $Cu(BF_4)_2\cdot xH_2O$ (0.083 g, 2.67×10^{-4} mol) in MeCN (20 cm^3) was stirred at room temperature for 30 min, yielding a deep green solution which was filtered and reduced to *ca*. 3 cm^3 volume. Vapour diffusion of Et_2O into this solution afforded large dark green blocks. Yield 0.13 g, 61%.

Crystallography

Single crystals of X-ray quality of complexes **1** and **2** were grown by diffusion of Et_2O into CH_2Cl_2 solutions of the complexes. Suitable single crystals of **7** were grown by vapour diffusion of Et_2O into a solution of the complex in MeCN. Experimental details from the structure determinations are given in Table 7. All structures were solved by direct methods (SHELXTL PLUS[49]) and refined by full-matrix least squares on F^2 (SHELXL 93[50]), with H atoms placed in calculated positions.

Complex 1·0.5H_2O. During refinement, the BF_4^- anion of the structure was found to be disordered, and was modelled by partial fluorine site occupancies such that the total number of F atoms equalled 4. In addition, a weakly scattering feature that was not bonded to either the cation or anion was modelled as half a molecule of lattice water. This result, which suggests that the lattice CH_2Cl_2 present in freshly prepared samples (Table 1) had exchanged with ambient moisture during the (4 month long) storage of the crystals, was confirmed by microanalysis of the sample employed in the X-ray experiment (Found: C, 58.0; H, 4.25; N, 13.9. Calc. for $C_{43}H_{37}B_2CuF_4N_9O_2\cdot0.5H_2O$: C, 58.6; H, 4.35; N, 14.3%). All non-H atoms with site occupancies ≥0.5, except the solvent O atom, were modelled anisotropically.

Complex 2·2CH_2Cl_2. During refinement, the BF_4^- anion of the structure was found to be disordered about the B(11)–F(11)

vector, and was modelled as for complex **1**. In addition, one of the two CH_2Cl_2 solvent molecules was modelled with chlorine atoms disordered over two orientations in a 7:3 occupancy ratio. All wholly occupied non-H atoms, together with the major orientation of the disordered solvent molecule, were modelled anisotropically.

Complex 7. During refinement, one of the two BF_4^- anions of the structure was found to be disordered, and was modelled as for complex **1**. All non-H atoms with site occupancies $\geqslant 0.5$ were modelled anisotropically. The high *R* factor for this structure is caused by poor crystal quality, which was observed consistently between different samples (the refinement reported here is the best from four data sets collected at room and low temperatures) and is reflected in the low number of observed reflections (Table 7).

Atomic coordinates, thermal parameters, and bond lengths and angles have been deposited at the Cambridge Crystallographic Data Centre (CCDC). See Instructions for Authors, *J. Chem. Soc*., *Dalton Trans*., 1997, Issue 1. Any request to the CCDC for this material should quote the full literature citation and the reference number 186/485.

Other measurements

Infrared spectra were obtained as Nujol mulls pressed between KBr windows, or in NaCl solution cells, between 4000 and 400 cm^{-1} using a Perkin-Elmer Paragon 1000 spectrophotometrer, UV/VIS spectra with a Perkin-Elmer Lambda 12 spectrophotometer operating between 1100 and 200 nm, in 1 cm quartz cells, NMR spectra on a Bruker DPX250 spectrometer, operating at 250.1 (^{1}H) and 62.9 MHz (^{13}C), electron-impact and positive-ion fast atom bombardment mass spectra on a Kratos MS50 spectrometer, the FAB spectra employing a 3-nitrobenzyl alcohol matrix. The microanalyses (C, H, N) were performed by the University of Cambridge Department of Chemistry microanalytical service. Melting points are uncorrected. The EPR spectra were obtained using a Bruker ESP300E spectrometer; for X-band a ER4102ST resonator and ER4111VT cryostat were employed, while for S-band spectra a ER4118SM-S-5W1 resonator and a ER4118VT cryostat were used. Spectral simulations were performed using in-house software which has been described elsewhere.[51] All electrochemical measurements were carried out using an Autolab PGSTAT20 voltammetric analyser, in MeCN or CH_2Cl_2 containing 0.1 and 0.5 mol dm^{-3} $NBu^n_4PF_6$ (prepared from NBu^n_4OH and HPF_6), respectively, as supporting electrolyte. Cyclic voltammetric experiments involved the use of a double platinum working/counter electrode and a silver-wire reference electrode; all potentials quoted are referenced to an internal ferrocene–ferrocenium standard and were obtained at a scan rate of 100 mV s^{-1}. The number of electrons involved in a given voltammetric process was determined by comparison of the peak height in the CV with that of the Fe^{II}–Fe^{III} couple shown by an equimolar amount of ferrocene.

Acknowledgements

The authors thank the Royal Society (London) for a University Research Fellowship (to M. A. H.), the EPSRC, the University of Cambridge and St. Catharine's College for financial support.

References

1 J. Stubbe, *Annu. Rev. Biochem*., 1989, **58**, 257; D. P. Goldberg and S. J. Lippard, *Adv. Chem. Ser*., 1995, **246**, 61; M. Fontecave and J.-L. Pierre, *Bull. Soc. Chim. Fr*., 1996, **133**, 653.
2 H. Sigel and A. Sigel (Editors), *Met. Ions. Biol. Syst*., 1994, **30**.
3 J. W. Whittaker, in ref. 2, p. 315; J. P. Klinman, *Chem. Rev*., 1996, **96**, 2541.
4 A. M. English and G. Tsaprailis, *Adv. Inorg. Chem.*, 1995, **43**, 79.
5 N. Ito, S. E. V. Phillips, C. Stevens, Z. B. Ogel, M. J. McPherson, J. N. Keen, K. D. S. Yadav and P. F. Knowles, *Nature* (*London*), 1991, **350**, 87.
6 A. J. Baron, C. Stevens, C. Wilmot, K. D. Seneviratne, V. Blakeley, D. M. Dooley, S. E. V. Phillips, P. F. Knowles and M. J. McPherson, *J. Biol. Chem*., 1994, **269**, 25 095.
7 J. M. Johnson, H. B. Halsall and W. R. Heineman, *Biochemistry*, 1985, **24**, 1579.
8 M. DeFillipis, C. P. Murthy, M. Faraggi and M. H. Klapper, *Biochemistry*, 1989, **28**, 4847.
9 M. M. Whittaker, W. R. Duncan and J. W. Whittaker, *Inorg. Chem*., 1996, **35**, 382.
10 M. A. Halcrow, H. R. Powell and M. J. Duer, *Acta Crystallogr*., *Sect. B*, 1996, **52**, 746.
11 D. L. Jameson, J. K. Blaho, K. T. Kruger and K. A. Goldsby, *Inorg. Chem*., 1989, **28**, 4312; D. L. Jameson and K. A. Goldsby, *J. Org. Chem*., 1990, **55**, 4992; D. L. Christenson, C. J. Tokar and W. B. Tolman, *Organometallics*, 1995, **14**, 2148; A. T. Baker, D. C. Craig, G. Dong and A. D. Rae, *Aust. J. Chem*., 1995, **48**, 1071.
12 M. Bruix, J. de Mendoza and J. Elguero, *Tetrahedron*, 1987, **43**, 4663.
13 R. J. Less, J. L. M. Wicks, N. P. Chatterton, M. J. Dewey, N. L. Cromhout, M. A. Halcrow and J. E. Davies, *J. Chem. Soc*., *Dalton Trans*., 1996, 4055.
14 N. Kitajima and W. B. Tolman, *Prog. Inorg. Chem.*, 1995, **43**, 419.
15 J. Perkinson, S. Brodie, K. Yoon, K. Mosny, P. J. Carroll, T. V. Morgan and S. J. Nieter Burgmayer, *Inorg. Chem*., 1991, **30**, 719.
16 M. A. Halcrow, J. E. Davies and P. R. Raithby, *Polyhedron*, 1997, **16**, 1535.
17 S. Trofimenko, J. C. Calabrese and J. S. Thompson, *Inorg. Chem.*, 1987, **26**, 1507; D. M. Eichhorn and W. H. Armstrong, *Inorg. Chem*., 1990, **29**, 3607.
18 J. C. Calabrese, P. J. Domaille, S. Trofimenko and G. J. Long, *Inorg. Chem*., 1991, **30**, 2795.
19 S. Trofimenko, J. C. Calabrese, J. K. Kochi, S. Wolowiec, F. B. Hulsbergen and J. Reedijk, *Inorg. Chem*., 1992, **31**, 3943.
20 S. Trofimenko, *J. Am. Chem. Soc*., 1967, **89**, 3170.
21 S. Trofimenko, *J. Am. Chem. Soc*., 1967, **89**, 6288.
22 A. Murphy, B. J. Hathaway and T. J. King, *J. Chem. Soc*., *Dalton Trans*., 1979, 1646.
23 N. Kitajima, Y. Moro-oka, A. Uchida, Y. Sasada and Y. Ohashi, *Acta Crystallogr*., *Sect. C*, 1988, **44**, 1876; R. E. Marsh, *Acta Crystallogr*., *Sect. C*, 1989, **45**, 1269.
24 S. G. N. Roundhill, D. M. Roundhill, D. R. Bloomquist, C. Landee, R. D. Willett, D. M. Dooley and H. B. Gray, *Inorg. Chem*., 1979, **18**, 831.
25 D. A. Bardwell, J. C. Jeffrey, P. L. Jones, J. A. McCleverty and M. D. Ward, *J. Chem. Soc*., *Dalton Trans*., 1995, 2921.
26 A. G. Orpen, L. Brammer, F. H. Allen, O. Kennard, D. G. Watson and R. Taylor, *J. Chem. Soc*., *Dalton Trans*., 1989, S1.
27 C. A. Hunter and J. K. M. Sanders, *J. Am. Chem. Soc*., 1990, **112**, 5525.
28 M. A. Halcrow, N. L. Cromhout and P. R. Raithby, unpublished work.
29 G. N. La Mar, W. DeW. Horrocks, jun. and R. H. Holm (Editors), *NMR of Paramagnetic Molecules*, Academic Press, New York, 1973, p. 678.
30 A. P. Kalverda, J. Salgado, C. Dennison and G. W. Canters, *Biochemistry*, 1996, **35**, 3085.
31 J. Foley, D. Kennefick, D. Phelan, S. Tyagi and B. J. Hathaway, *J. Chem. Soc*., *Dalton Trans*., 1983, 2333; H. Nakai, *Bull. Chem. Soc. Jpn*., 1983, **56**, 1637.
32 M. A. Halcrow, unpublished work.
33 F. Santavy, D. Walterová and L. Hruban, *Collect. Czech. Chem. Commun*., 1972, **37**, 1825.
34 M. Kahn and J. B. Polya, *J. Chem. Soc. C*, 1970, 85.
35 B. J. Hathaway, in *Comprehensive Coordination Chemistry*, eds. G. Wilkinson, R. D. Gillard and J. A. McCleverty, Pergamon, Oxford, 1987, vol. 5, ch. 53, pp. 662–679.
36 A. B. P. Lever, *Inorganic Electronic Spectroscopy*, Elsevier, Amsterdam, 2nd edn., 1984, pp. 554–572.
37 A. B. P. Lever, *J. Chem. Educ*., 1974, **51**, 612.
38 M. Kasha, H. R. Rawls and M. Ashraf El-Bayoumi, *Pure Appl. Chem*., 1965, **11**, 371.
39 J. Vasudevan, R. T. Stibrany, J. Bumby, S. Knapp, J. A. Potenza, T. J. Emge and H. J. Schugar, *J. Am. Chem. Soc*., 1996, **118**, 11 676 and refs. therein.
40 B. A. Goodman and J. B. Raynor, *Adv. Inorg. Chem*., 1970, **13**, 135.

41 A. Zweig, W. G. Hodgson and W. H. Jura, *J. Am. Chem. Soc*., 1964, **86**, 4124.
42 O. S. Musgrave and C. J. Webster, *J. Chem. Soc. C*, 1971, 1397; K. Bechgaard and V. D. Parker, *J. Am. Chem. Soc*., 1972, **94**, 4749; V. Le Berre, J. Simonet and P. Batail, *J. Electroanal. Chem. Interfacial Electrochem.*, 1984, **169**, 325; V. Le Berre, L. Angely, N. Simonet-Gueguen and J. Simonet, *New J. Chem*., 1985, **9**, 419.
43 J. A. Cowan and J. K. M. Sanders, *J. Chem. Soc*., *Perkin Trans. 1*, 1987, 2395.
44 S. B. Ferguson, E. M. Seward, F. Diederich, E. M. Sanford, A. Chou, P. Inocencio-Szweda and C. B. Knobler, *J. Org. Chem*., 1988, **53**, 5593; C. A. Hunter, M. N. Meah and J. K. M. Sanders, *J. Am. Chem. Soc*., 1990, **112**, 5773; H. L. Anderson, C. A. Hunter, M. N. Meah and J. K. M. Sanders, *J. Am. Chem. Soc*., 1990, **112**, 5780; J. Zhang and J. S. Moore, *J. Am. Chem. Soc*., 1992, **114**, 9701.
45 (*a*) S. K. Burley and G. A. Petsko, *Science*, 1985, **229**, 23; (*b*) W. L. Jorgensen and D. L. Severance, *J. Am. Chem. Soc*., 1990, **112**, 4768.
46 F. Cozzi, M. Cinquini, R. Annunziata, T. Dwyer and J. S. Siegel, *J. Am. Chem. Soc*., 1992, **114**, 5729.
47 W. R. Scheidt, K. E. Brancato-Buentello, H. Song, K. V. Reddy and B. Cheng, *Inorg. Chem*., 1996, **35**, 7500.
48 A. J. Amoroso, A. M. Cargill Thompson, J. C. Jeffrey, P. L. Jones, J. A. McCleverty and M. D. Ward, *J. Chem. Soc*., *Chem. Commun*., 1994, 2751.
49 G. M. Sheldrick, SHELXTL PLUS, PC version, Siemens Analytical Instruments Inc., Madison, WI, 1990.
50 G. M. Sheldrick, SHELXL 93, University of Göttingen, 1993.
51 F. E. Mabbs and D. Collison, *Electron Paramagnetic Resonance of d Transition Metal Compounds*, Elsevier, Amsterdam, 1992, ch. 7.

Received 14*th January* 1997; *Paper* 7/03376A